




# Analysis of Spontaneous Ignition of Grass: Chemical Oxidation and Water Vapor Sorption

R. Font <sup>\*</sup>, Department of Chemical Engineering, University Institute of Chemical Process Engineering, University of Alicante, Apto 99, Alicante, Spain

**Received:** 14 June 2021/**Accepted:** 30 November 2021/**Published online:** 16 December 2021

**Abstract.** Self-heating of biomass by chemical oxidation, which can cause spontaneous ignition, is a safety and management concern. This process can be accelerated by aerobic fermentation and water vapor sorption. The chemical oxidation and water vapor sorption of grass were studied in a laboratory oven, measuring the variations in weight and the internal temperature of a sphere with grass within a flexible polymeric network. Both processes were simulated to prove that the proposed mathematical model could fit the experimental data. It was observed that the water vapor sorption capacity of the grass was high, so the experimental increase in the internal temperature of a spherical body was around 47 K, from 73°C to 120°C. This fact can be very important because the chemical oxidation of grass accelerates at high temperatures. For scaling, simulation programs were used to study the sorption and oxidation processes with an increase in internal temperature in spherical bodies and infinite plane slabs. These results can be used to obtain those of other geometric symmetries by interpolation. It was deduced that at 70°C and with vapor sorption, the ignition time can be around 3 days to 5 days, while without vapor sorption, the ignition times can be around 110 days to 140 days. For 35°C the ignition times with vapor sorption can be around 12 days to 18 days, while without vapor sorption the ignition times can be around 3700 days to 4500 days. These results can be of interest for warehouses of similar biomass and for forestry research and management groups of wild-fires. Graphical Abstract

**Keywords:** Ignition, Self-heating, Water vapor sorption, Chemical oxidation, Kinetics, Grass

## List of Symbols

$C_p$	Specific heat in J/kg K
$D_{\text{eff}}$	Effective diffusivity in $\text{m}^2/\text{s}$
$E_{\text{ox}}$	Apparent activation energy of the oxidation reaction in J/kmol
$k_{\text{eff}}$	Effective internal thermal conductivity in W/m K
$K_x$	Mass transfer coefficient in $\text{kg water}/(\text{s m}^2 (\text{kg water}/\text{kg air}))$
$\Delta H_{\text{ox}}$	Heat of the oxidation reaction in J/kg
$h$	Heat transfer coefficient in $\text{W}/\text{m}^2 \text{ K}$

<sup>\*</sup>Correspondence should be addressed to: R. Font, E-mail: [rafael.font@ua.es](mailto:rafael.font@ua.es), [rafael.fontmontesinos@gmail.com](mailto:rafael.fontmontesinos@gmail.com)



NCV	Neat calorific value in J/kg
R	Gas constant in J/kmol K.
r	Radius of the sphere in m,
SIT	Self-ignition temperature in °C or K
T	Temperature in °C or K
$t_{ad}$	Adiabatic induction period in s
X	Ratio in kg water + kg d.s./kg initial d.s
$\delta_{critical}$	Critical dimensionless parameter for runaway, used in Eq. (1)
$\rho_s$	Density of the solids or bulk density in kg/m <sup>3</sup>

## 1. Introduction

The understanding of the causes and conditions of spontaneous ignition is the subject of research in literature. Spontaneous ignition, or self-ignition, is sometimes the last step of a self-heating process, occurring due to different exothermic processes, such as aerobic digestion, water vapor sorption and chemical oxidation [1].

The risk of self-ignition is important for biomass, raw materials (grains, milk powders, etc.) and wastes (shells, grain and powders, sludge, etc.). It was discussed that self-heating leading to self-ignition can occur by aerobic fermentation and/or vapor water sorption followed by chemical oxidation in a large quantity of material [1–5]. Here, the heat generated by any mechanism is greater than the heat lost to the environment, and consequently, the temperature increases continuously until ignition.

Grass has a significant water vapor sorption capacity, and it also undergoes chemical oxidation. Therefore, this study may be interesting, considering that grass is also a component of forests and could be the initial cause of wildfires. Grass and similar biomass materials can be stored in heaps or inside warehouses. In addition to grass, there are herbs, straws and shrubs in forests which can accumulate in an area. This topic can be interesting for forestry research and management groups. These accumulations can potentially cause fires due to a temperature rise via the mechanisms introduced above in some special cases. The analysis carried out can be applied to all wastes with a high capacity of water vapor sorption. It must be noted that liquid sorption also causes a rise in temperature, but this increase is less than with vapor water [6]. On the other hand, coals also have the ability to adsorb water vapor and increase self-heating and the possibilities of runaway (uncontrolled increases in temperature), so the procedure used can be useful for the study of carbonaceous materials.

Numerous works have analyzed self-ignition on the basis of the Frank–Kamenetskii theory applied to different bodies (spheres, cubes, slabs, etc.). For a body with a characteristic length (radius, height, thickness) and constant parameters (such as the activation energy, kinetic factor (including terms of fuel and oxygen concentrations), oxidation enthalpy and effective internal heat conductivity), the temperature of the outer surface is critical to runaway. For temperatures of the external surface less than the critical temperature, the body can reach a pseudo-stationary state where there is a stable temperature gradient between the maximum temperature at the center of the body and the outer surface [7–19].

The critical ambient temperature  $T_{a,critical}$  (given in Kelvin), which coincides with the external surface temperature, is also called the self-ignition temperature (SIT) and leads to runaway [20]. It can be defined by:

$$\delta_{critical} = \frac{\Delta H_{ox} E_{ox} r^2 k_{ox} \rho_s}{k_{eff} R T_{a,critical}^2} \exp\left(-\frac{E_{ox}}{R T_{a,critical}}\right) \quad (1)$$

The critical dimensionless parameter,  $\delta_{critical}$ , takes the value of 3.32 for a sphere.  $\Delta H_{ox}$  is the heat of the oxidation reaction in J/kg,  $E_{ox}$  is the apparent activation energy of the oxidation reaction in J/kmol,  $k_{ox}$  is the kinetic factor of the reaction in  $s^{-1}$ ,  $\rho_s$  is the density of the solids or bulk density in  $kg/m^3$ ,  $k_{eff}$  is the effective internal thermal conductivity in W/m K,  $r$  is the radius of the sphere in meters, and  $R$  is the gas constant in J/kmol K.

From Eq. (1), the following equation is derived, which forms the basis for the EN15188 test method.

$$\ln \frac{\delta_{critical} T_{a,critical}^2}{r^2} = \ln \frac{\Delta H_{ox} E_{ox} k_{ox} \rho_s}{R k_{eff}} - \frac{E_{ox}}{R T_{a,critical}} \quad (2)$$

On the other hand, it is possible to estimate the time necessary to runaway when there is no loss of heat to the surroundings, that is, in an adiabatic process. This time is known as the adiabatic induction period of time,  $t_{ad}$ , and is defined as follows:

$$\frac{1}{t_{ad}} = \frac{\Delta H_{ox} k_{ox}}{C_p} \frac{E_{ox}}{R T_o^2} \exp\left(-\frac{E_{ox}}{R T_o}\right) \quad (3)$$

In Eq. (3),  $T_o$  is the initial temperature of the body in Kelvin and  $C_p$  is the specific heat. The adiabatic induction time is less than that of the real process, where a fraction of the heat generated is lost to the surroundings. However, it does give an indication because the real adiabatic induction time for runaway to occur in the real process is greater than  $t_{ad}$ .

The objective of this research was to analyze chemical oxidation and sorption of water vapor on grass (material with a high capacity for water sorption), to study their propensity of spontaneously combust, and to scale the oven experimental data to big bodies. Methods developed elsewhere [1] have been applied to the material used to study both water vapor sorption and chemical oxidation, both separately and, at times, simultaneously. Simulation programs were also used to fit to the experimental results and to extrapolate the process for large bodies, where the ambient temperature can be low, or close to room temperature.

## 2. Material and Methods

### 2.1. Material

The material used (*Stenotaphrum secundatum*) was obtained from the collection piles of cut grass from the University of Alicante gardens. Table 1 shows the chemical and physical characterization of the material used.

Elemental analysis was determined using the Perkin-Elmer 2400 apparatus. The NCV (Net Calorific Value) was obtained using the AC-350 LECO calorimetric bomb. As shown in Table 1, the oxygen content is 24.4% (calculated as the difference between 100 and the total percentage of carbon, hydrogen, nitrogen and ash combined). The ash content was determined using an oven at 550°C. The specific heat value was determined by the hot water process in an adiabatic vessel, and the determined value is within the range of those proposed in the literature for different types of biomass [21]. The surface area determined by Multi-point BET with nitrogen is 1.2 m<sup>2</sup>/g. The real density determined with water is 747 kg/m<sup>3</sup>, so the porosity range taking into account the bulk density is 0.82 to 0.97. The moisture content at room conditions is around 0.1 kg water/kg d.s..

### 2.2. Apparatus

A diagram of the apparatus used can be found elsewhere [1]. The MEMMERT oven had a cavity with the following dimensions: 32 cm × 24 cm × 17.5 cm. Inside the laboratory oven, spherical samples with a diameter between 4 cm and 13 cm were placed inside an inert cubic mesh but maintaining the spherical shape or in a ball formed by the grass contained in an inert polymeric network with 2 cm orifices, allowing the flux of gases and retaining and pressing the material. The two blowers were made and inserted into the oven by laboratory personnel.

The weight variation was measured using an Ohaus Pyoneer balance, with a sensitivity of 0.001 g. The internal temperature of the samples and the temperature of the oven were measured with K-chromel–alumel thermocouples with a sensitivity of 1°C placed in the center of the body and inside the oven respectively [1].

**Table 1**  
**Characterization of Grass**

Elemental analysis wt% (dry solid)		Bulk properties	
C	42.2	Bulk density	23.6–132 kg/m <sup>3</sup>
H	4.9	Heat capacity	1309 J/kg K
N	3.6	Effective or bulk thermal conductivity	0.0550 W/m K
O	24.4 (by difference)	Net calorific value (NCV)	1.447 × 10 <sup>7</sup> J/kg
Ash	24.9		

### 2.3. Methods

Spherical samples were selected for symmetry within the furnace and their ease of data processing. Some experimental runs were duplicated in the most significant cases, such as the weight loss due to the oxidation and the water vapor sorption at 70°C. Temperature measurements were made simultaneously with the weight loss measurements. With the introduction of the thermocouple into the sample, there was a slight variation in weight and then there was no longer an appreciable influence.

The method used to determine the convective heat transfer coefficient was similar to that shown elsewhere [1]. With wet pieces of aluminum foil were inside a polymeric network forming a 7.0 cm diameter sphere, the heat transfer coefficient was 13.4 W/m<sup>2</sup> K.

The value of the effective or bulk thermal conductivity of the grass inside the spherical body was determined from the simulation of the runs carried out to analyze the chemical oxidation. The simulation also considered the heating and cooling processes of the samples where the heat transfer predominates at temperatures less than 120°C, when the chemical oxidation is negligible. The effective thermal conductivity value was 0.0550 W/m K, which minimizes the differences between the experimental and calculated values. A detailed analysis is carried out in Sect. 3.3. Thermal conductivity was also determined by a modified transient plane source (MTPS) method, determining the thermal effusivity [22]. The values obtained for non-ground and ground (to 2 mm diameter particles) and pressed grass samples were 0.0442 and 0.0683 W/m K, respectively. These values are close to the value 0.0550 W/m K of the effective thermal conductivity determined from the comparison between the experimental and calculated values of non-ground samples (Sect. 3.3). All the experimental runs presented in the following section were carried out with non-ground samples.

Water vapor sorption was determined using dry, spherical samples formed on a polymeric network. These samples were placed on a rack above a balance to record the weight gain. Through two curved tubes, hot water was introduced into the aluminum foil trays located at the bottom of the oven, generating an atmosphere with a high water vapor concentration inside the oven. Liquid water had no contact with the sample. In the spherical body, there was a considerable increase in temperature within the sample. When the initial hot water temperature was higher than the oven temperature, the water temperature dropped rapidly to the oven temperature and then very slowly to 10°C to 15°C below the oven temperature. The humidity was maintained at 100% during the first part of the experimental run and then was slowly decreased to 80% to 70%. In the experiments where the initial temperature of the hot water was equal to the oven temperature, the temperature was very slowly decreased to 10°C to 15°C below the oven temperature, with humidity from 100% to 70% to 60%. For the experiments carried out at temperatures higher than 100°C, the partial pressure of water was around 340 mm Hg to 500 mm Hg. Equilibrium was reached when a constant weight was reached. The decrease in the temperature of the hot water is due to its vaporiza-

tion to maintain the humidity, which decreases as a consequence of the vapor sorption of the sample.

The chemical oxidation of the material was measured by the decrease in weight of the spherical samples within the polymeric network while also measuring the internal temperature.

The simulation program used, along with Excel spreadsheets, is similar to that indicated in [1], both without, and with, water vapor sorption. When applied to a spherical body, the simulation considers 20 elements with the same dry solid mass, the mass and energy balances for each element, the mass and heat flows, and the temperature increase due to water vapor sorption and chemical oxidation.

### 3. Results and Discussion

#### 3.1. Experimental Values and Analysis of Water Vapor Sorption

Different tests were carried out with grass in order to observe the increase in temperature inside spherical samples, when hot water was introduced inside the oven. Figure 1 shows the results of an experimental run carried out with 31.2 g of dry material in a 13 cm diameter sphere (density of  $27 \text{ kg/m}^3$ ). An increase in moisture can be observed from practically 0 to 0.10 kg water/kg dry solid when hot water at  $85^\circ\text{C}$  was added to the foil trays. The internal temperature of the grass sample went from  $71^\circ\text{C}$ , which was the temperature of the stabilized oven, to  $112^\circ\text{C}$ , showing an increase of 41 K. Subsequently, the temperature slowly dropped to the oven temperature. It was also observed that the initial moisture increase is very fast, coinciding with the temperature peak, and then it slowly increases until the final moisture content is reached. Liquid water was not in contact with the sample. These experimental runs were carried out using samples of three different sizes and adding the hot water at  $71^\circ\text{C}$  or  $85^\circ\text{C}$  (with possible formation of small drops). Similar moisture curves and temperature peaks to those

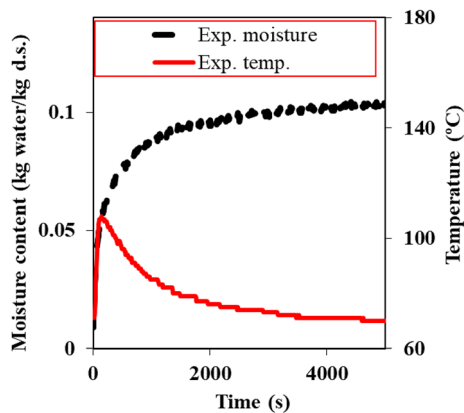


**Figure 1. Sorption of water vapor in a low density ball of grass (density 27 of  $\text{kg/m}^3$ ).**

shown in Fig. 1 were obtained. Table 2 shows the temperature increases of these experimental runs.

In the experimental runs carried out with the smallest grass spheres, the addition of hot water at 85°C resulted in the moisture rising to 0.127 and then decreasing to around 0.1 kg water/kg dry solid. This trend could probably be explained by the consequence of an initial water condensation at the outer layers followed by water sorption, whereas for the larger grass sphere, the condensation did not take place as intensively, because the outer layers are less significant with respect to the whole particle.

In order to determine the relative importance of the two phenomena (condensation and water sorption), a denser ball of slightly compressed grass was prepared, as this may correspond to real samples in bales, stacks or other situations containing compressed material. This sample compression minimizes the phenomena of water condensation with respect to vapor sorption. The sorption of water vapor in saturated surroundings is also complicated by condensation, and for this reason, equilibrium data of many substances are only determined from 0% to 95% relative humidity [23–27].

A 7.0 cm diameter grass sphere was prepared within an inert polymeric network to study the vapor sorption at 73°C, after the addition of hot water at around 85°C to the aluminum foil trays. Here, the water temperature dropped to around 75°C and then slowly decreased further to 55°C to 65°C. The density of this ball was 132 kg/m<sup>3</sup>. All the following data presented in this paper, both experimental and simulated data, refer to these spherical balls with a density of 132 kg/m<sup>3</sup> (this is higher than those used to obtain the data in Fig. 1 where the spheres had a low density of 27 kg/m<sup>3</sup>). Figure 2 shows the variation in the moisture in the solid, and the internal temperature.

To ensure the relatively large increase of 47 K was correct, the experimental run was repeated and the result was the same.

Note that the exothermic condensation and mainly the sorption process cause the increase in temperature to a peak, but the exothermic sorption process continues with the increase in moisture.

**Table 2**  
**Final Moisture Content and Changes in Temperature due to Sorption of Water by Samples of Grass Without Any Compression (Oven Temperature = 71 °C)**

Diam. (cm)	Mass (g) dry solid	Density (kg/m <sup>3</sup> )	Moisture after adding hot water at 71°C		Moisture after adding hot water at 85°C	
			(kg water/kg dry solid)	Temperature increase K	(kg water/kg dry solid)	Temperature increase K
7	5.061	28.2	0.105	21	0.127–0.097	30
9	9.026	23.6	0.106	33	0.127–0.108	40
13	31.172	27.1	0.103	35	0.104	41

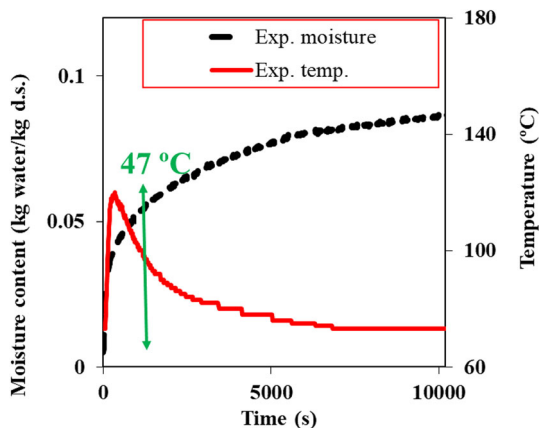


**Figure 2. Variation in moisture content and temperature versus time for the water adsorption run carried out at 73°C (density of 132 kg/m<sup>3</sup>).**

Lohrer et al. [28, 29] also studied the influence of liquid and water vapor sorption on the self-ignition with German lignite coal. In an experimental run with 100 ml, the rise in temperature in the center of the sample was 33 K, from 77°C to 110°C, when the relative humidity was increased from 18% to 99%. The shape of the variation in the experimental temperature is similar to that shown in Fig. 2, but there is no data on the moisture variation of the solid.

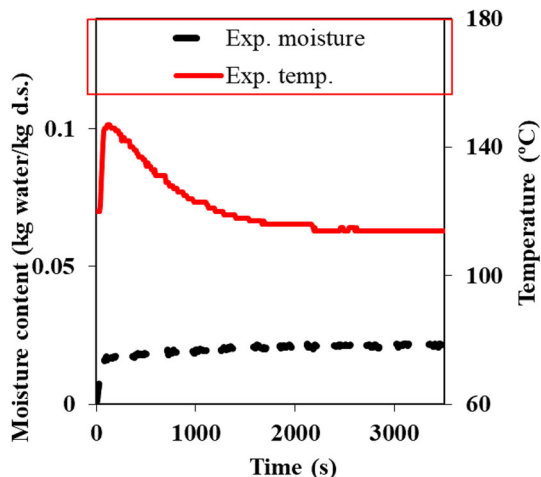
Miura [27] observed an increase in temperature from 38°C to over 60°C with samples of pre-dried and cooled coal (100 mg) when exposed to saturated air at 38°C, concluding the importance of water sorption in the spontaneous heating. The shape of the variation in the experimental temperature is also similar to that shown in Fig. 2, but there is no data on the moisture variation of the solid.

Fu et al. [5] presents the temperature increase inside a eucalyptus bark pile due to the water vapor as the ambient humidity increases, emphasizing the importance of vapor sorption favoring spontaneous ignition.

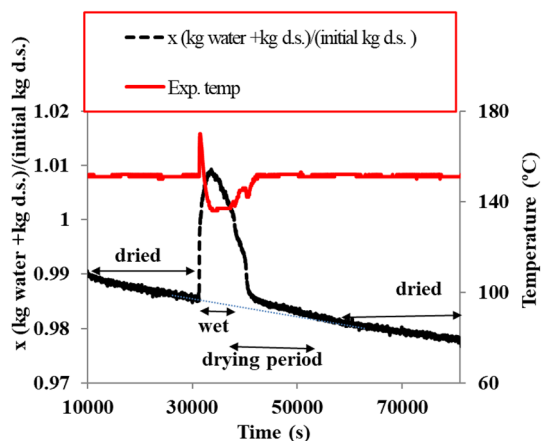
Figure 3 shows the results obtained in the experimental run with an initial temperature of 120°C and a final temperature of 114°C. However, in this case, the temperature increase in the center was 27 K. This is less than the 47 K change seen with the experimental run carried out at 73°C due to less water being adsorbed.

Figure 4 shows another water adsorption experimental run performed using a 7.0 cm diameter sphere (23.6 g) and an initial high temperature of 152°C, coinciding with the oven temperature that was maintained quasi-constant during the run. After adding hot water to the aluminum foil trays, the internal temperature rose to a peak at 170°C, and then decreased to 138°C. The temperature of the hot water added was around 85°C during the period of time considered in the experimental run. The ratio ((kg water + kg dry solid)/initial dry solid) versus time was used to assess the water adsorption and the initial decrease in weight prior to the





**Figure 3. Variation in moisture content and temperature versus time for the water sorption run carried out at 120-114°C (density of 132 kg/m<sup>3</sup>).**



**Figure 4. Variation in X (kg water + kg d.s.)/kg initial d.s. versus time for a run with initial temperature of 152°C (density of 132 kg/m<sup>3</sup>).**

addition of hot water, as a consequence of chemical oxidation. The estimated value for the sorption capacity at 138°C was evaluated at the moisture peak observed in Fig. 4, which was the objective of this complex run. Nevertheless, the sorption capacity is low (around 0.0237 kg water/kg dry solid).

For different oven temperatures, Fig. 5 shows the moisture content corresponding to the equilibrium with water vapor versus the sample temperature, deducing

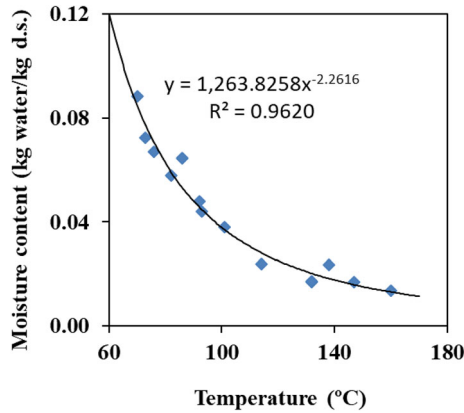


**Figure 5. Estimated values of equilibrium moisture versus temperature.**

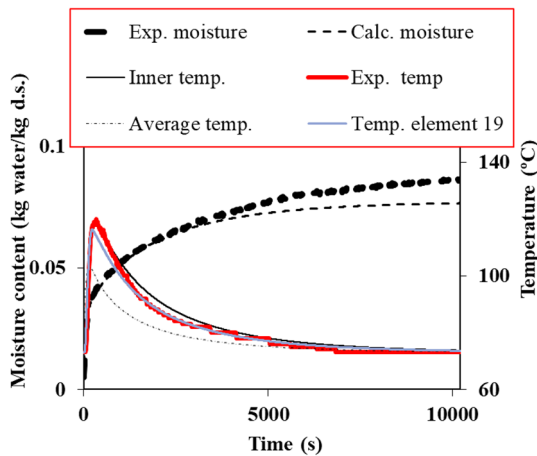


**Figure 6. Variation in moisture and temperature for the run carried out at 73°C: experimental and calculated values (density of 132 kg/m<sup>3</sup>).**

a decreasing variation as expected. These data must be considered as an estimate of water sorption for high values of air humidity.

### 3.2. Simulation of the Water Sorption Process

The simulation program used was similar to that shown in [1]. The simulation is complex considering the mass and heat transfer and also taking into account that the moisture content cannot be greater than the equilibrium content. The enthalpy of sorption is also assumed to be equal to the enthalpy of condensation at the corresponding temperature.

Figure 6 shows the simulated results of the experimental run performed at 73°C. The variation in the moisture in the sample and the internal temperatures of two elements are also shown. The two elements considered are the inner element at the center of the body (element 20) and the element adjacent to the center (element 19). The values of the heat transfer coefficient, 13.4 W/m<sup>2</sup> K, and effective thermal conductivity 0.0550 W/ m K, were those presented previously. The mass transfer coefficient  $K_x$  and the effective diffusivity were determined to obtain an acceptable fit of the experimental data, with the values of  $K_x$  and the effective diffusivity  $D_{\text{eff}}$  taken to be 0.00958 kg water/(s m<sup>2</sup> (kg water/kg air)) and  $7.710 \times 10^{-7}$  m<sup>2</sup>/s, respectively.

It can be seen that the simulation is satisfactory for the first part of the simulated run, but the final moisture cannot be obtained with the equilibrium data considered. Figure 7 presents the simulated results when the equilibrium data of the moisture is increased by a factor of 1.1 to  $1.1 \times 1263(T)^{-2.2616}$  (where T is given in °C). In this case, the simulation is satisfactory for the entire simulated run. Although there is a small deviation in the moisture-time variation in the first part of the simulated run, the variation of temperature is similar to that shown in Fig. 6.

Figures 8 and 9 show the simulated results corresponding to the variation shown in Fig. 7. Figure 8 also shows the variation in the moisture in both the external and internal elements, showing the corresponding differences. Figure 9 shows the variation in moisture content with respect to temperature, with the variation in equilibrium for different elements. It can be observed that there is an initial period with increasing variation in moisture and temperature to reach the equilibrium curve, and from this point onwards, the variations are equal to those shown by the equilibrium curve. The simulated results are in accordance with the

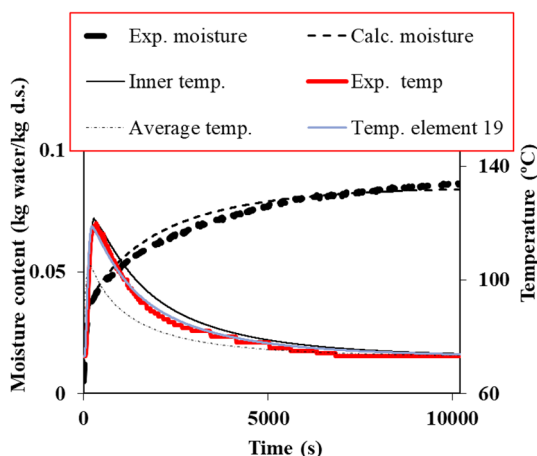


**Figure 7. Variation in moisture and temperature versus time for the run carried out at 73°C, increasing the sorption capacity by a factor 1.1 (density of 132 kg/m<sup>3</sup>).**

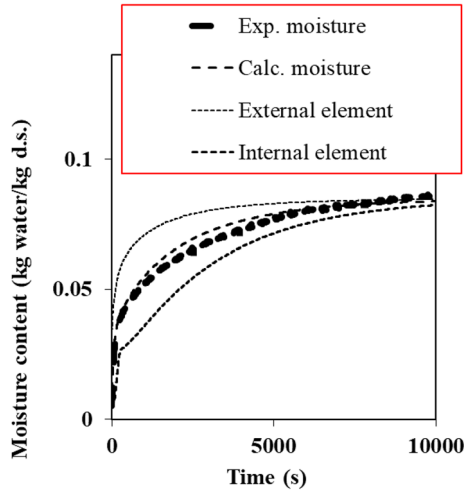


**Figure 8. Variation in moisture and temperature for the run carried out at 73°C: experimental value and calculated values for external and internal elements (density of 132 kg/m<sup>3</sup>).**

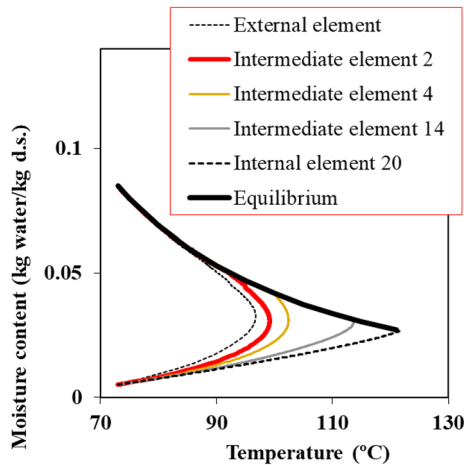


**Figure 9. Simulated variation in moisture versus temperature for the run carried out at 73°C (density of 132 kg/m<sup>3</sup>).**

initial hypothesis included in the simulation program, but the detailed variation can be observed.

Lohrer et al. [28] have numerically simulated the temperature variation in the center of the 100 ml German lignite sample with water vapor sorption, also obtaining variations in the experimental and simulated values similar to those shown in Fig. 6.

Fu et al. [5] have deduced numerically a temperature rise from 30°C to 74°C when varying the ambient humidity in a eucalyptus bark pile, showing the importance of water vapor sorption and favoring the microbiological activity and the chemical reaction in the days following the temperature rise.

### 3.3. Kinetics of the Process

The oxidation kinetics was deduced from different experimental runs carried out at different temperatures by measuring the weight loss over a long period of time, either with or without the addition of hot water. The reaction rate was calculated from the constant linear variation in the relative weight loss with respect to the initial mass versus time, taking into account that the oxidation degree is small. In the experimental runs carried out at high temperatures, blackening of the sample was observed, showing carbonization as in many processes with the release of carbon oxides. The kinetics determined at different temperatures is analyzed considering the global reaction that implies a weight loss. Figure 10 shows the variation in the reaction rate with respect to the inverse of the absolute temperature. Only two runs with vapor sorption were performed to confirm that there is not a significant influence on the thermal oxidation, one at 122°C with 341 mm Hg vapor pressure and the other at 152°C with water vapor sorption with 450 mm Hg vapor pressure as indicated in Fig. 4.

Vance et al. [30] studied the effect of the moisture content on the spontaneous combustion of coal, observing that at low moisture contents of 4.5 and 5.5%, the temperature–time profiles during spontaneous heating are similar, although the data are not compared with dry samples.

The value of the slope and, consequently the apparent activation energy are similar to those derived with almond shells using the same apparatus and procedure [1]. The value of apparent activation energy is 94 kJ/mol, which is a value close to the activation energies obtained by different authors with biomass and

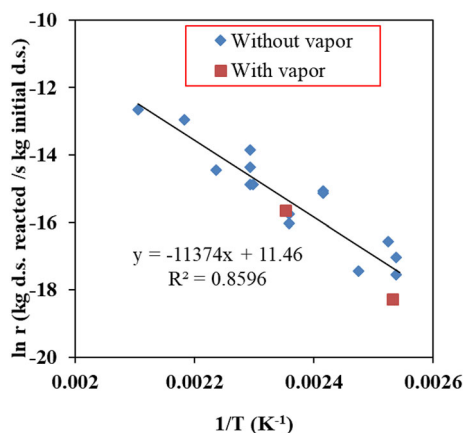


**Figure 10. Variation in the reaction rate versus the inverse of absolute temperature.**

some types of coal (85 kJ/mol to 99 kJ/mol) [14, 16, 31], but less than the value obtained with other types of coal (105 kJ/mol to 139 kJ/mol) [7, 11, 14, 16]. Note that the similarities are a consequence of a similar oxidation process with the lignocellulosic compounds.

Schwarzer et al. [32] studied the low temperature oxidation of biomass from 150°C to 250°C, obtaining an apparent activation energy of 130 kJ/mol for the lumped volatilizable component (extractives + hemicellulose + lignin + cellulose). Wang et al. [33] analyzed the mechanism of the low-temperature oxidation of coal below 100°C, considering two parallel reactions, direct burn-off and chemisorption sequence. Considering the similarity of the apparent activation energy between biomass and carbon, it is possible that the mechanisms were similar, although this aspect deserves to be investigated.

Figure 11 shows the experimental results of the temperature variation in a 7.0 cm diameter grass ball over time in a long experimental multi-step run with

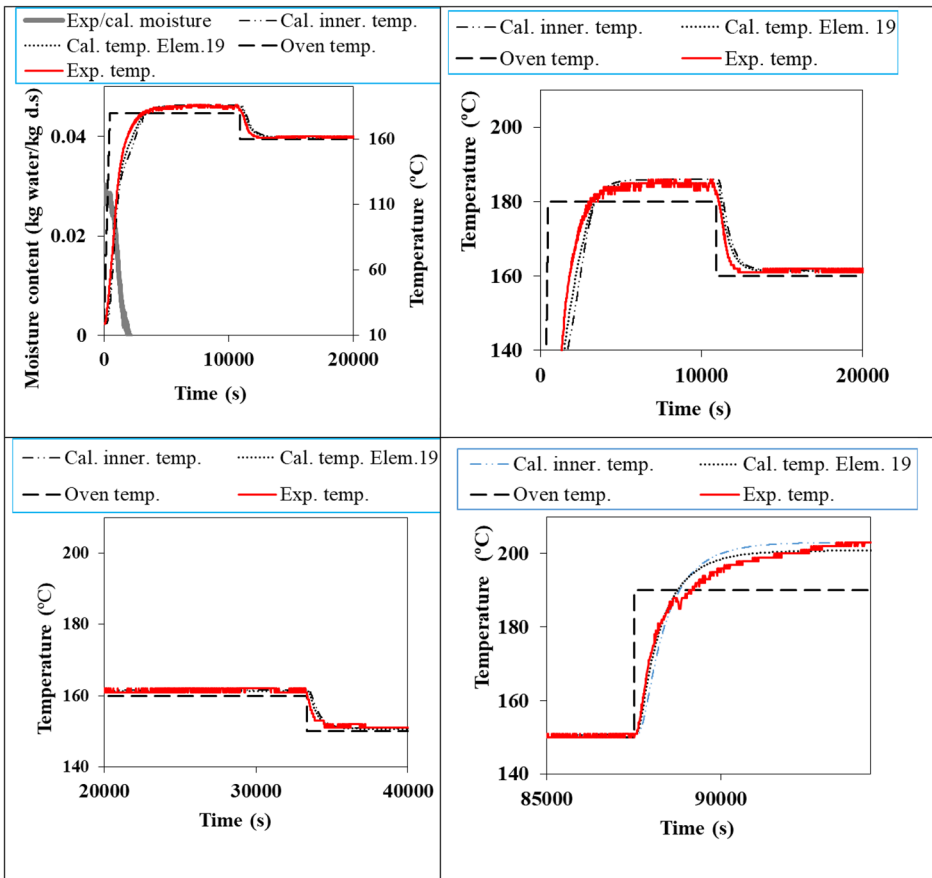


**Figure 11. Variation in moisture content and temperature for a long run carried out at different temperatures (density of 132 kg/m<sup>3</sup>).**

different final temperatures. In this run, the initial temperature was low, and during the heating stage controlled by the oven taking into account the temperature inside the oven and the set temperature, the sample was dried. The simulated results were obtained with the same simulation program. The values of  $C_p$  and  $h$  were 1309 J/kg K and 13.4 W/m<sup>2</sup> K, respectively. The value of the mass transfer coefficient was  $9.58 \times 10^{-3}$  kg water/s m<sup>2</sup> (kg water/kg dried air) and the value of the internal diffusion was  $3333 \times \exp(-10,000/T)$  kg water/(s m<sup>2</sup>(kg water/m<sup>3</sup>)). This part of the simulation does not interfere with the vapor sorption and the oxidation processes considered in this research.

Considering mainly the data from 8000 s onwards (after the drying process), the effective thermal conductivity  $k_{\text{eff}}$  value was deduced from the comparison between the experimental variation in the temperature over time, with the one deduced by simulation. The optimal  $k_{\text{eff}}$  value was obtained where the agreement between experimental and calculated variations was the best. This optimal  $k_{\text{eff}}$  value was 0.0550 W/m K, a value inside the interval deduced by thermal effusivity (0.0442 W/m K to 0.0683 W/m K) as commented previously [22].

On the other hand, it can be observed that after a period of time, the experimental internal temperature is higher than the oven temperature as a consequence of the exothermic oxidation reaction. A reaction enthalpy value  $\Delta H_{\text{ox}}$  of  $6.584 \times 10^6$  J/kg (around 45.5% of the NCV) was also deduced, considering the rise in temperature with respect to the oven temperature. A good fitting with the deduced parameters can be observed considering the variation in elements 20 or inner temperature and element 19, adjacent to the inner element. Note that in these experimental runs, the increase in temperature of the inner element is determined when a pseudo stationary state was reached. Probably, with an ambient temperature of 193°C to 194°C the runaway would be reached. The proposed method can be useful to analyze the self-ignition without the need to reach a fire inside the oven.

### 3.4. Self-heating Analysis Considering the Maximum Temperature Rise

In this section, the same analysis performed in the previous almond shells study [1] was used on the grass samples and the results are presented. In a case without runaway, the spherical body, after a long period, reaches a pseudo-steady state with a temperature gradient between the outer surface and the center of the sphere. From a heat balance and taking into account the heat evolved in the chemical oxidation, the deduced equations useful for the analysis of the temperature rise are the following:

$$T_{\text{center}} - T_{\text{outer}} = \frac{T_{\text{center}} - T_{\text{ambient}}}{\left[1 + \frac{2k_{\text{eff}}}{hr}\right]} \quad (4)$$

and

$$\ln \left[ \frac{6(T_{\text{center}} - T_{\text{outer}})}{r^2} \right] \cong \ln \left[ \frac{\Delta H_{\text{ox}} \rho_s k_{\text{ox}}}{k_{\text{eff}}} \right] - \frac{E_{\text{ox}}}{RT_{\text{ave}}} \quad (5)$$

Estimated values of  $E_{\text{ox}}/R$  and the parameter  $\Delta H_{\text{ox}} \rho_s k_{\text{ox}}/k_{\text{eff}}$ , can be obtained for the characterization of self-heating and spontaneous combustion.

Table 3 shows the experimental results of the measured temperatures and the deduced parameters. The  $T_{\text{ave}}$  values have been calculated as  $0.8 \times T_{\text{center}} + 0.2 \times T_{\text{amb}}$ , taking into account the exponential variation in the heat released when the temperature changes.

Figure 12 shows the variation in  $\ln(6*(T_{\text{center}} - T_{\text{outer}})/(r^2))$  as a function of  $1/T_{\text{ave}}$ .

Figure 12 also shows the predicted variation in  $\ln(6*(T_{\text{center}} - T_{\text{outer}})/(r^2))$  with  $(1/T_{\text{ave}})$  according to Eq. 5 for different absolute temperatures. For the predicted variation,  $\Delta H_{\text{ox}}$  is taken to be  $6.584 \times 10^6$  J/kg,  $\rho_s$  is  $132$  kg/m<sup>3</sup>,  $k_{\text{ox}}$  is  $9.485 \times 10^4$  s<sup>-1</sup>,  $E/R$  is  $11374$  K and  $k_{\text{eff}}$  is  $0.0550$  W/m K. The values of  $\Delta H_{\text{ox}}$  and  $k_{\text{eff}}$  were derived from the simulation shown in Fig. 11, whereas the kinetic parameters  $k_{\text{ox}}$  and  $E_{\text{ox}}/R$  were deduced from the kinetics of weight loss shown in Fig. 10. The value of  $\Delta H_{\text{ox}} \rho_s k_{\text{ox}}/k_{\text{eff}}$  is  $1.502 \times 10^{15}$  K/m<sup>2</sup>. It can be seen in Fig. 12 that the two variations are close to each other.

Both  $E_{\text{ox}}/R$  values of  $11,374$  K (deduced from the weight variation shown in Fig. 10) and  $10,119$  K (deduced from the variations in temperature shown in Fig. 12, experimental points) are close, showing that the data, in spite of the differences in the  $E/R$  values, are consistent. The parameter  $\Delta H_{\text{ox}} \rho_s k_{\text{ox}}/k_{\text{eff}}$  deduced from the simulation runs is  $1.502 \times 10^{15}$  K/m<sup>2</sup>, while the value considering the variations in temperature increase is  $9.83 \times 10^{13}$  K/m<sup>2</sup>. These values of  $\Delta H_{\text{ox}} \rho_s k_{\text{ox}}/k_{\text{eff}}$  show a small, but significant difference, due to the differences in the  $E/R$  values.

From the analysis of the data and the relative incidence of the different parameter used, the most important factors in the increase in temperature are the mass of sample used, the  $C_p/k_{\text{eff}}$  ratio, the  $\Delta H_{\text{ox}} k_{\text{ox}}/k_{\text{eff}}$  ratio and the activation energy  $E_{\text{ox}}$ . Taking into account all the experimental errors, the parameters obtained can

**Table 3**  
**Experimental Temperatures and Calculation of Parameters (Mass Dry Solid = 0.2376 kg and Radius, r = 0.035 m)**

$T_{\text{amb}}$ (°C)	$T_{\text{center}}$ (°C)	$T_{\text{center}} - T_{\text{amb}}$ (K)	$T_{\text{center}} - T_{\text{outer}}$ (K)	$T_{\text{outer}}$ (°C)	$T_{\text{ave}}$ (K)	$6*(T_{\text{center}} - T_{\text{outer}})/$ $(r^2)$ (K/m <sup>2</sup> )
190	203	13	10.79	192.20	473.99	52,881
180	186	6	4.98	181.01	458.15	24,406
170	174	4	3.32	170.67	446.48	16,271
160	162	2	1.66	160.33	434.82	8135
150	151	1	0.83	150.16	423.98	4067



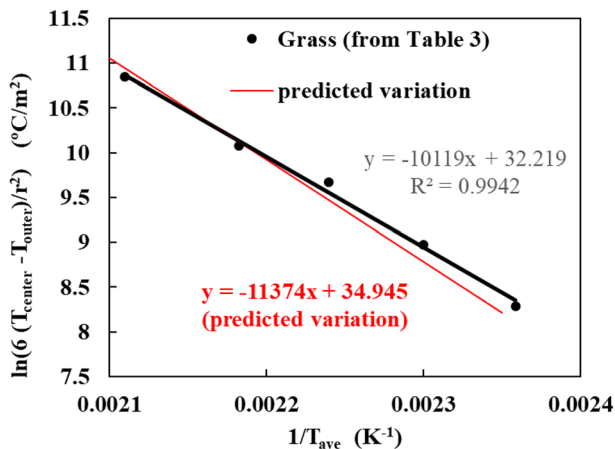


**Figure 12.** Variation in  $\ln(6(T_{center} - T_{outer})/r^2)$  versus  $1/T_{ave}$ .

be considered as values proposed with an error of around 10% to 15%. Nevertheless, the values are coherent as can be observed in Fig. 12, and they are useful to analyze the self-ignition process.

The self-heating and thermal runaway of four types of biomass without vapor sorption have also been studied by Schwarzer et al. [34] at the lab-scale and modelled satisfactorily, taking into account all the external and internal mass and heat transfer in cylindrical samples.

#### 4. Scaling

Two simulations programs have been used: (a) a new program considering an infinite plane slab and (b) a similar program considering a sphere [1]. The parameters considered were the same as those used previously in the experimental runs explained in the previous sections, where the mass transfer coefficient  $K_x$  for water vapor is taken as  $9.58 \times 10^{-3}$  kg water/(s  $m^2$  (kg water/kg dry air)) and the internal diffusion coefficient,  $D_{eff}$ , is  $7.710 \times 10^{-7}$   $m^2/s$ . To calculate the sorption equilibria, the moisture content is (kg water/kg d.s.) =  $1263 \times (\text{temperature in } ^\circ\text{C})^{-2.2316}$ , the heat transfer coefficient is  $13.4 \text{ W/m}^2 \text{ K}$ , the effective internal thermal conductivity is  $0.0550 \text{ W/m K}$ , the enthalpy of oxidation is  $6.584 \times 10^6 \text{ J/kg}$ , the pre-exponential kinetic factor is  $9.485 \times 10^4 \text{ s}^{-1}$  and the  $E_{ox}/R$  value is taken as  $11,374 \text{ K}$ . The influence of the external heat transfer is small, so the temperature of the outer element is close to the ambient temperature.

Figure 13 shows the variation in the radius of the sphere and the half-thickness of an infinite slab versus the critical temperature for ignition without and with vapor sorption.

The plotted points corresponding to the results without vapor sorption are those obtained by Eq. (1) when the ambient temperature equals the temperature of the external surface of the body. The values of  $\delta_{critical}$  for the sphere with

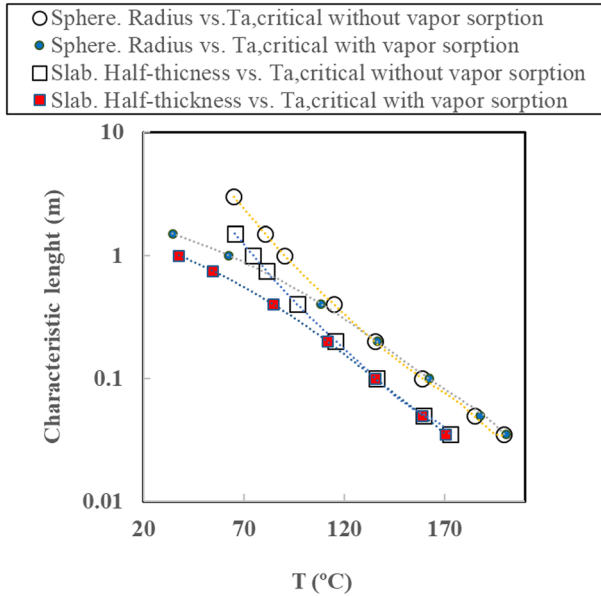


**Figure 13. Variation in the sphere radius and the slab half-thickness versus the critical ambient temperature.**

radius  $r$  and for the infinite plane slab of width  $2r$  are 3.32 and 0.878 respectively [20, 35]. The values of the critical temperatures have been tested with the simulation programs with an error less than  $0.5^{\circ}\text{C}$  to  $1^{\circ}\text{C}$  when considering high values of external heat transfer, such as  $100\text{ W/m}^2\text{K}$ . Considering the value of the individual heat transfer of  $13.4\text{ W/m}^2\text{K}$  used in the simulations carried out in this work, the incidence in the value of the critical temperature is less than  $2^{\circ}\text{C}$  to  $3^{\circ}\text{C}$  and only for small samples with sphere radius or half-thickness less than  $0.1\text{ m}$ .

The critical temperature obtained with water vapor sorption was estimated with an error of  $\pm 0.5^{\circ}\text{C}$ , so  $0.5^{\circ}\text{C}$  higher ignition was observed and  $0.5^{\circ}\text{C}$  lower ignition was not detected. Note that determining the critical temperature is not easy, because at the critical temperature, the time necessary to reach the ignition is infinite.

From Eq. (1), the following equation can be deduced:

$$\frac{r}{\delta_{\text{critical}}^{0.5}} = \left[ \frac{k_{\text{eff}}R}{\Delta H_{\text{Ox}}E_{\text{Ox}}k_{\text{Ox}}\rho_s} \right]^{0.5} T_{a,\text{critical}} \exp\left( \frac{E_{\text{ox}}}{RT_{a,\text{critical}}} \right) \tag{6}$$

This means that for different bodies and with the same physicochemical parameters, for the same critical ambient temperature  $T_{a,\text{critical}}$ , the same value of  $r/\delta_{\text{critical}}^{0.5}$  is obtained for different geometries. Consequently, considering the values of  $\delta_{\text{critical}}$  of 3.32 for a sphere and 0.878 for a slab, the same value of the critical tem-

perature corresponds to an infinite slab with a half-thickness  $r$  and for a sphere radius  $r/(3.32/0.878)^{0.5}$ , which means  $r/1.944$ .

According to the previous analysis, Fig. 14 shows the variation in  $r$  (half-thickness of a slab) and  $r$  (sphere radius)/1.944 versus the critical temperature for both cases without or with water vapor sorption.

The fitting equations for the Fig. 14 are shown in Table 4, considering the inverse of the absolute temperature.

The variations observed in Fig. 14 for the sphere and slab are close to each other. Note that for  $T_{a,critical}$  higher than  $110^{\circ}\text{C}$ , the incidence of the vapor sorption is very small or negligible compared to the results without vapor sorption. It can be observed that vapor sorption favors self-ignition by lowering the critical temperature for the same body size. This effect was experimentally observed by Lohrer et al. [28, 29] with German lignite coal.

Figure 15 shows the variation in the ignition times for different cases: without and with vapor sorption with a heat transfer coefficient of  $13.4 \text{ W/m}^2\text{K}$ , and the adiabatic case. Ignition times have been calculated at  $5^{\circ}\text{C}$  above the critical temperature, as shown in Fig. 13, for each value of half-thickness slab or sphere radius/1.944.

The equations obtained from the fitting of the simulated results of ignition times are shown in Table 5.

From Fig. 15, it can be observed that the variations deduced for the sphere and slab are close to each other. Without vapor sorption, both variations are above the variation corresponding to the adiabatic process, which is consistent due to the heat loss.

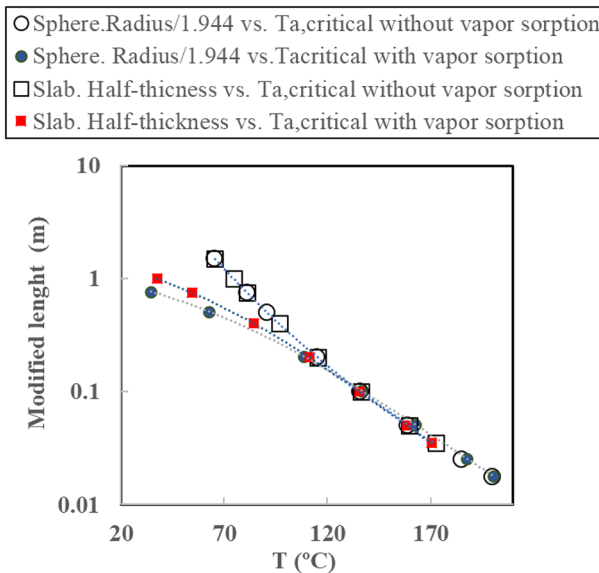


**Figure 14. Variation in the sphere radius/1.994 and the slab half-thickness versus the critical ambient temperature.**

**Table 4**  
**Fitting Equations: Variation of the Sphere Radius/1.994 and the Slab Half-Thickness Versus the Inverse of the Critical Ambient Temperature**

y = sphere radius/1.944 or infinite slab half-thickness (m)			
x = 1/T <sub>a,critical</sub> (K <sup>-1</sup> )			R <sup>2</sup>
<i>Without vapor sorption</i>			
From Eq. (1) and simulation:	$y = 2.414 \times 10^{-7} \exp(5298x)$ (7)		0.9999
Exact solution from Eq. (4)	$y = 2.267 \times 10^{-10} x \exp(5687x)$ (8)		
<i>With vapor sorption, with heat transfer coefficient = 13.4 W/m<sup>2</sup>K</i>			
Sphere	$y = -2.861 \times 10^8 x^3 + 2.740 \times 10^6 x^2 - 7.770 \times 10^3 x + 6.905$ (9)		0.9998
Infinite plane slab	$y = -2.765 \times 10^8 x^3 + 3.071 \times 10^6 x^2 - 9.519 \times 10^3 x + 9.055$ (10)		0.9999

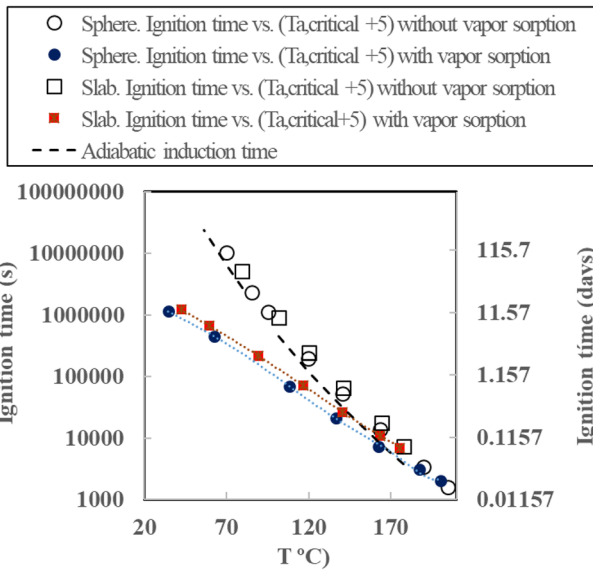


**Figure 15. Variation in the ignition times versus temperature: without and with vapor sorption.**

The simulated adiabatic ignition times calculated are 6% to 10% greater than those calculated by the approximate Eq. (3).

It can be deduced that with vapor sorption the ignition time is much shorter than without vapor sorption.

Table 6 shows the corresponding sizes for different geometries and the ignition times, taking into account that the two geometries analyzed, infinite slab and

**Table 5**  
**Variation in Ignition Time Versus the Inverse of the Critical Temperature**

$y = \text{Ignition time (s)}$ $x = 1/T_{a,\text{critical}} \text{ (K}^{-1}\text{)}$		$R^2$
<i>Without vapor sorption with heat transfer coefficient of 13.4 W/m<sup>2</sup>K:</i>		
Sphere	$y = 4.217 \times 10^{-7} \exp(10556x) \quad (11)$	0.9999
Infinite plane slab	$y = 6.152 \times 10^{-7} \exp(10503x) \quad (12)$	0.9997
<i>Without vapor sorption in an adiabatic process (heat transfer coefficient = 0)</i>		
Adiabatic ignition time: sphere and slab	$y = 2.400 \times 10^{-7} \exp(10572x) \quad (13)$	0.9994
<i>With vapor sorption, with heat transfer coefficient of 13.4 W/m<sup>2</sup>K</i>		
Sphere	$y = 1.142 \times 10^{15}x^3 - 7.749 \times 10^{12}x^2 + 1.754 \times 10^{10}x - 1.325 \times 10^7 \quad (14)$	0.9999
Infinite plane slab	$y = 1.771 \times 10^{15}x^3 - 1.229 \times 10^{13}x^2 + 2.851 \times 10^{10}x - 2.212 \times 10^7 \quad (15)$	0.9999

sphere, represent the two extreme values of  $\delta_{\text{critical}}$ , giving close results. Table 6 also shows the comparison factor for the different geometries, so  $r$  for infinite slab and  $r/\text{comparison factor}$  is the value  $y$  for Eqs. (8–10). For the critical temperature 65°C without vapor sorption, the dimensions for the different bodies have been calculated by Eq. (8). The values shown are the exact values. The ignition times for 70°C (5°C above the critical temperature) without vapor sorption have been calculated by Eq. (11) for the sphere and Eq. (12) for the infinite slab. For the rest of the geometries, the estimated values have been obtained by linear interpolation between the two extremes values, slab and sphere, and considering the values of  $\delta_{\text{critical}}$ .

For vapor sorption with heat transfer coefficient of 13.4 W/m<sup>2</sup>K, the dimension  $r$  is calculated by Eq. (9) for the sphere, Eq. (10) for the slab and by interpolation for the remaining geometries considering the values of  $\delta_{\text{critical}}$ . For the calculation of the ignition time with vapor sorption, Eq. (14) for the sphere and Eq. (15) for the slab have been used, and for the other geometries the ignition times are obtained by interpolation considering the values of  $\delta_{\text{critical}}$ .

From Table 6 (ambient temperature 70°C), it can be observed that the ignition times with vapor sorption (3 days to 5 days) are much shorter than when there is no vapor sorption (110 days to 140 days).

Table 7 shows the results for geometries with dimensions corresponding to a critical temperature of 30°C and with an ambient temperature of 35°C. It can be deduced that without vapor sorption the ignition times are very long (3700 days to 4500 days), which indicates that only by self-heating, final self-ignition is unlikely to occur. However, with vapor sorption, ignition times can be about 12 days to 18 days. These results can be considered as an estimate that mainly indicates

**Table 6**  
**Values of the Dimensions for Different Geometries for a Critical Ambient Temperature of 65°C and Ignition Times for an Ambient Temperature of 70°C**

Geometry	Dimensions	$\delta_{critical}$ [20, 35]	Factor = $\frac{(\delta_{cri})}{0.878}^{0.5}$	Without vapor sorption		With vapor sorption		
				Size for $T_{a,critical} = 65 + 273$ K	Ignition time at 70°C (days)	y	Size for $T_{a,critical} = 65 + 273$ K	Ignition time at 70°C (days)
Infinite plane slab	Width $2r$	0.878	1.000	$r = 1.544$ m	139	0.6110	$r = 0.6110$ m	4.86
Infinite square rod	Side $2r$	1.7	1.391	$r = 1.544 \times 1.391 = 2.148$ m	130	0.5703	$r = 0.5703 \times 1.391 = 0.7933$ m	4.47
Rectangular box	Sides $2l, 2r, 2m$ $l = r = m/10$	1.75	1.412	$l = r = 1.544 \times 1.412 = 2.180$ m $m = 10 \times 1.544 \times 1.412 = 21.80$ m	129	0.5679	$l = r = 0.5679 \times 1.412 = 0.8018$ m $m = 10 \times 0.5679 \times 1.412 = 8.018$ m	4.44
Infinite cylinder	Radius $r$	2	1.509	$r = 1.544 \times 1.509 = 2.330$ m	126	0.5555	$r = 0.5555 \times 1.509 = 0.8338$ m	4.32
Cube	Side $2r$	2.52	1.694	$r = 1.544 \times 1.694 = 2.615$ m	120	0.5298	$r = 0.5298 \times 1.694 = 0.8974$ m	4.07
Equicylinder	Radius $r,$ height $2r$	2.76	1.773	$r = 1.544 \times 1.773 = 2.737$ m	117	0.5179	$r = 0.5179 \times 1.773 = 0.9182$ m	3.96
Sphere	Radius $r$	3.32	1.944	$r = 1.544 \times 1.944 = 3.001$ m	111	0.4902	$r = 0.4902 \times 1.944 = 1.188$ m	3.69

**Table 7**  
**Values of Dimensions for Different Geometries for a Critical Ambient Temperature of 30°C and Ignition Times for an Ambient Temperature of 35°C**

Geometry	Dimensions	$\delta_{critical}$ [20, 35]	Without vapor sorption			With vapor sorption		
			Factor	Size for $T_{a,critical} = 30 + 273$ K	Ignition time at 35°C (days)	y	Size for $T_{a,critical} = 30 + 273$ K	Ignition time at 35°C (days)
Infinite plane slab	Width 2r	0.878	1.000	r = 9.646 m	4519	1.147	r = 1.147 m	17.32
Infinite square rod	Side 2r	1.7	1.391	r = 9.646 × 1.391 m = 13.42 m	4236	1.037	r = 1.037 × 1.391 m = 1.442 m	15.74
Rectangular box	Sides 2 l, 2r, 2 m l = r = m/10	1.75	1.412	l = r = 9.646 × 1.412 = 13.62 m m = 10 × 9.646 × 1.412 = 136.2 m	4219	1.030	lr = 1.030 × 1.412 = 1.459 m = 10 × 1.030 × 1.412 = 14.59 m	15.65
Infinite cylinder	Radius r	2	1.509	r = 9.646 × 1.509 = 14.56 m	4133	0.997	r = 0.997 × 1.509 = 1.504 m	15.17
Cube	Side 2r	2.52	1.694	r = 9.646 × 1.694 = 16.34 m	3954	0.927	r = 0.927 × 1.694 = 1.570 m	14.17
Equicylinder	Radius r, height 2r	2.76	1.773	r = 9.646 × 1.773 = 17.10 m	3871	0.895	r = 0.895 × 1.773 = 1.586 m	13.71
Sphere	Radius r	3.32	1.944	r = 9.646 × 1.944 = 18.75 m	3678	0.820	r = 1.594 × 1.944 = 1.594 m	12.64

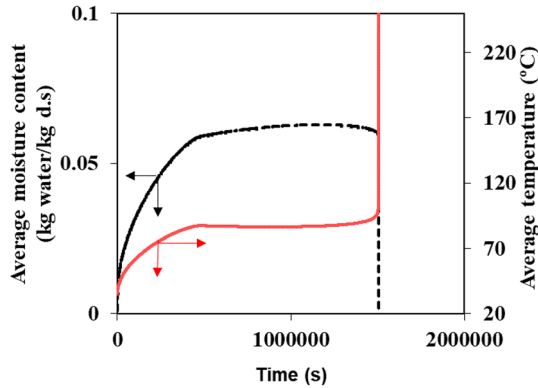


**Figure 16. Variation in moisture and temperature versus time for an infinity plane slab with half-thickness of 1.147 m, ambient temperature of 35°C and ignition time of 17.4 days.**

the significant influence of vapor sorption, accelerating self-heating of the grass leading to self-ignition.

Figure 16 shows the results for the infinite slab with half-thickness of 1.147 m and an ambient temperature of 35°C with the rest of the parameters indicated in the first paragraph of this section. The ignition time is 17.4 days and note that there is an increase in the moisture to approximately 0.062 kg water /kg d.s, causing an increase in the average temperature from 35°C to about 86°C and, consequently favoring the chemical oxidation that leads to self-ignition. Note that water vapor diffusion was considered in all cases, whereas it was assumed that oxygen gradient effect was negligible.

The above results discuss the significant influence that vapor sorption can cause on self-ignition. In warehouses or in forests, the environmental conditions can be very different to those indicated in this paper, and the temperature rise may not be as great. Fortunately, self-ignition cannot easily happen and special conditions must be met. Solar radiation can help increase the temperature and dry the material, so it can also favor the subsequent sorption of water vapor from the humidity of the air or from humid gases given off in fermentations. Climate change with an increase in environmental temperature can favor both processes: initial drying and oxidation.

On the other hand, the analysis carried out without or with water vapor sorption, can be useful the assessment and quantification of fire risk, in a manner similar to that presented by Restuccia et al. [7] in carbon-rich soils and Yuan et. al. [36] in peat where the biological process was also considered.



## **5. Conclusions**

The knowledge of the causes of self-heating and self-ignition in warehouses with ligno-cellulosic materials and forests is interesting to reduce the risk of fires. Grass is a waste or material that can be stored for animal feed, composting and fuel, and similar ligno-cellulosic materials are present in forests. Though runs carried out in a laboratory oven, chemical oxidation and water vapor sorption were studied.

With 7 cm diameter grass spheres, increases in internal temperature were observed from 50°C to higher temperatures and the weight loss was determined from 120°C to 180°C, deducing an activation energy around 94 kJ/mol by two independent methods.

Grass also has a considerable water vapor sorption capacity, which is why a large increase in temperature of the internal part of a 7.0 cm diameter dry spherical body was observed in an experiment when hot water was introduced into the oven. This increase was approximately 47 K from 73°C to 120°C.

By scaling, the significant incidence of the vapor sorption was observed by greatly shortening the ignition times from months to days. It was deduced that at 70°C and with vapor sorption, the ignition time can be around 3 days to 5 days and at 35°C the ignition times with vapor sorption can be around 12 days to 18 days. These data can be interesting to analyze the risk of fires and mainly when there is a change in the air humidity.

## **Acknowledgements**

Thanks are due to Daniel Agustín Ortiz de la Morena and Ana Isabel Moreno Caballero for their help in the implementation of the equipment, and to Alicia Font Escamilla for her help in correcting the work. Funding is from the University of Alicante.

## **Funding**

Open Access funding provided thanks to the CRUE-CSIC agreement with Springer Nature.

## **Open Access**

This article is licensed under a Creative Commons Attribution 4.0 International License, which permits use, sharing, adaptation, distribution and reproduction in any medium or format, as long as you give appropriate credit to the original author(s) and the source, provide a link to the Creative Commons licence, and indicate if changes were made. The images or other third party material in this article are included in the article's Creative Commons licence, unless indicated

otherwise in a credit line to the material. If material is not included in the article's Creative Commons licence and your intended use is not permitted by statutory regulation or exceeds the permitted use, you will need to obtain permission directly from the copyright holder. To view a copy of this licence, visit <http://creativecommons.org/licenses/by/4.0/>.

## References

1. Font R (2020) Analysis of the spontaneous combustion and self-heating of almond shells. *Fuel*. <https://doi.org/10.1016/j.fuel.2020.118504>
2. Krigstin S, Wetzel S (2016) A review of mechanisms responsible for changes to stored woody biomass fuels. *Fuel* 175:75–86. <https://doi.org/10.1016/j.fuel.2016.02.014>
3. Li XR, Koseki H, Momota M (2006) Evaluation of danger from fermentation-induced spontaneous ignition of wood chips. *J Hazard Matter A* 135:15–20. <https://doi.org/10.1016/j.hazmat.2005.11.034>
4. Zambra CE, Moraga NO, Escudey M (2011) Heat and mass transfer in unsaturated porous media: moisture effects in compost piles self-heating. *Int J Heat Mass Transf* 54:2801–2810. <https://doi.org/10.1016/j.heatmasstransfer.2011.01.031>
5. Fu S, Chen HX, Watt SD, Sidhu HS, Luangwilai T, Shu YF (2021) Numerical study on effect of ambient humidity variation on self-heating and spontaneous ignition of the eucalyptus bark pile. *Fire Technol*. <https://doi.org/10.1007/s10694-021-01091-4>
6. Fu ZM, Koseki H, Iwata Y (2006) Investigation on spontaneous ignition of two kinds of organic material with water. *Thermochim Acta* 440:68–74. <https://doi.org/10.1016/j.tca.2005.10.010>
7. Restuccia F, Huang XY, Rein G (2017) Self-ignition of natural fuels: can wildfires of carbon-rich soil start by self-heating?. *Fire Saf J* 91:828–834. <https://doi.org/10.1016/j.firesaf.2017.03.052>
8. Wu DJ, Huang XY, Norman F, Verplaetsen F, Berghmans J, Van den Bulck E (2015) Experimental investigation on the self-ignition behaviour of coal dust accumulations in oxy-fuel combustion system. *Fuel* 160:245–254. <https://doi.org/10.1016/j.fuel.2015.07.050>
9. Wu DJ, Norman F, Schmidt M, Vanierschot M, Verplaetsen F, Berghmans J et al (2017) Numerical investigation on the self-ignition behaviour of coal dust accumulations: the roles of oxygen, diluent gas and dust volume. *Fuel* 188:500–510. <https://doi.org/10.1016/j.fuel.2016.10.063>
10. Wu DJ, Schmidt M, Huang XY, Verplaetsen F (2017) Self-ignition and smoldering characteristics of coal dust accumulations in O<sub>2</sub>/N<sub>2</sub> and O<sub>2</sub>/CO<sub>2</sub> atmospheres. *Proc Combust Inst* 36(2):3195–3202. <https://doi.org/10.1016/j.proci.2016.08.024>
11. Wang YJ, Zhang XM, Sugai Y, Sasaki K (2017) Determination of critical self-ignition temperature of low-rank coal using a 1 m wire-mesh basket and extrapolation to industrial coal piles. *Energy Fuel* 31(7):6700–6710. <https://doi.org/10.1021/acs.energy-fuels.7b00409>
12. Janes A, Carson D, Accorsi A, Chaineaux J, Tribouilloy B, Morainvillers D (2008) Correlation between self-ignition of a dust layer on a hot surface and in baskets in an oven. *J Hazard Mater* 159(2–3):528–535. <https://doi.org/10.1016/j.jhazmat.2008.02.057>
13. Garcia-Torrent J, Ramirez-Gomez A, Querol-Aragon E, Grima-Olmedo C, Medic-Pejic L (2012) Determination of the risk of self-ignition of coals and biomass materials. *J Hazard Mater* 213:230–235. <https://doi.org/10.1016/j.jhazmat.2012.01.086>

14. Schmidt M, Wanke C, Krause U (2013) Determination of measurement uncertainties in adiabatic hot-storage experiments for reactive dusts. *Chem Eng Technol* 36(10):1764–1772. <https://doi.org/10.1002/ceat.201300068>
15. Veznikova H, Perdochova M, Bernatik A, Binkau B (2014) Safe storage of selected fuels with regard to their tendency to spontaneous combustion. *J Loss Prevent Proc* 29:295–299. <https://doi.org/10.1016/j.jlp.2014.03.011>
16. Binkau B, Wanke C, Krause U (2015) Influence of inert materials on the self-ignition of flammable dusts. *J Loss Prevent Proc* 36:337–344. <https://doi.org/10.1016/j.jlp.2014.11.017>
17. Pejic LM, Anez NF, Torrent JG, Ramirez-Gomez A (2015) Determination of spontaneous combustion of thermally dried sewage sludge. *J Loss Prevent Proc* 36:354–359. <https://doi.org/10.1016/j.jlp.2015.01.013>
18. Ferrero F, Lohrer C, Schmidt BM, Noll M, Malow M (2009) A mathematical model to predict the heating-up of large-scale wood piles. *J Loss Prevent Proc* 22(4):439–448. <https://doi.org/10.1016/j.jlp.2009.02.009>
19. Ramirez A, Garcia-Torrent J, Tascon A (2010) Experimental determination of self-heating and self-ignition risks associated with the dusts of agricultural materials commonly stored in silos. *J Hazard Mater* 175(1–3):920–927. <https://doi.org/10.1016/j.jhazmat.2009.10.096>
20. Gray BF (2016) Spontaneous-combustion and self-heating. In: Hurley M (ed) *SFPE handbook of fire protection engineering*, 5th edn. Springer, New York, pp 604–632
21. Dupont C, Chiriac R, Gauthier G, Toche F (2014) Heat capacity measurements of various biomass types and pyrolysis residues. *Fuel* 115:644–651. <https://doi.org/10.1016/j.fuel.2013.07.086>
22. Jensen CU, Guerrero JKR, Karatzos S, Olofsson G, Iversen SB (2017) Fundamentals of hydrofaction(TM): renewable crude oil from woody biomass. *Biomass Convers Bioresour* 7(4):495–509. <https://doi.org/10.1007/s13399-017-0248-8>
23. Guo X, Wu YQ, Xie XF (2017) Water vapor sorption properties of cellulose nanocrystals and nanofibers using dynamic vapor sorption apparatus. *Sci Rep* 7:14207. <https://doi.org/10.1038/s41598-017-14664-7>
24. Hill CAS, Norton A, Newman G (2009) The water vapor sorption behavior of natural fibers. *J Appl Polym Sci* 112(3):1524–1537. <https://doi.org/10.1002/app.29725>
25. Sghaier K, Peczalski R, Bagane M (2018) Water sorption equilibria and kinetics of henna leaves. *Heat Mass Transf* 54(5):1545–1554. <https://doi.org/10.1007/s00231-017-2237-7>
26. Vasquez VR, Coronella CJ (2009) A simple model for vapor–moisture equilibrium in biomass substrates. *Aiche J* 55(6):1595–1603. <https://doi.org/10.1002/aic.11762>
27. Miura K (2016) Adsorption of water vapor from ambient atmosphere onto coal fines leading to spontaneous heating of coal stockpile. *Energy Fuel* 30(1):219–229. <https://doi.org/10.1021/acs.energyfuels.5b02324>
28. Lohrer C, Krause U, Steinbach J (2005) Self-ignition of combustible bulk materials under various ambient conditions. *Process Saf Environ* 83(B2):145–150. <https://doi.org/10.1205/psep.0423>
29. Lohrer C, Schmidt A, Krause U (2005) A study on the influence of liquid water and water vapour on the self-ignition of lignite coal-experiments and numerical simulations. *J Loss Prevent Proc* 18(3):167–177. <https://doi.org/10.1016/j.jlp.2005.03.006>
30. Vance WE, Chen XD, Scott SC (1996) The rate of temperature rise of a subbituminous coal during spontaneous combustion in an adiabatic device: the effect of moisture content and drying methods. *Combust Flame* 106(3):261–270. [https://doi.org/10.1016/0010-2180\(95\)00276-6](https://doi.org/10.1016/0010-2180(95)00276-6)

31. Chong LV, Chen XD, Mackereth AR (1999) Effect of ageing and composition on the ignition tendency of dairy powders. *J Food Eng* 39(3):269–276
32. Schwarzer L, Sarossy Z, Jensen PA, Glarborg P, Karlstrom O, Holm JK, Dam-Johansen K (2019) Kinetic parameters for biomass under self-ignition conditions: low-temperature oxidation and pyrolysis. *Energy Fuel* 33(9):8606–8619. <https://doi.org/10.1021/acs.energyfuels.9b00848>
33. Wang H, Dlugogorski BZ, Kennedy EM (2003) Analysis of the mechanism of the low-temperature oxidation of coal. *Combust Flame* 134(1–2):107–117. [https://doi.org/10.1016/S0010-2180\(03\)00086-5](https://doi.org/10.1016/S0010-2180(03)00086-5)
34. Schwarzer L, Jensen PA, Wedel S, Glarborg P, Karlstrom O, Holm JK, Dam-Johansen K (2021) Self-heating and thermal runaway of biomass? Lab-scale experiments and modeling for conditions resembling power plant mills. *Fuel* . <https://doi.org/10.1016/J.Fuel.2021.120281>
35. Bowes PC (1971) Application of the theory of thermal explosion to the self-heating and ignition of organic materials. In: *F. R. N.*, p 867
36. Yuan H, Restuccia F, Rein G (2021) Spontaneous ignition of soils: a multi-step reaction scheme to simulate self-heating ignition of smouldering peat fires. *Int J Wildland Fire* 30(6):440–453. <https://doi.org/10.1071/WF19128>

**Publisher's Note** Springer Nature remains neutral with regard to jurisdictional claims in published maps and institutional affiliations.